Case Studies in Thermal Engineering 26 (2021) 101029

Contents lists available at ScienceDirect

Case Studies in Thermal Engineering

journal homepage: www.elsevier.com/locate/csite

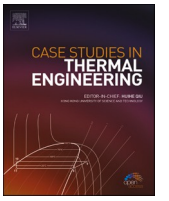

Experimental study on the thermal performance of a battery thermal management system using heat pipes

Hussein Mbulu [a], Yossapong Laoonual [a], Somchai Wongwises [a,b,*]

[a] Fluid Mechanics, Thermal Engineering and Multiphase Flow Research Lab (FUTURE), Department of Mechanical Engineering, Faculty of Engineering, King Mongkut's University of Technology Thonburi, Bangmod, Bangkok, Thailand
[b] National Science and Technology Development Agency (NSTDA), Pathum Thani, 12120, Thailand

ARTICLE INFO

Keywords:
Electric vehicle
Battery thermal management system
Water cooling
Heat pipe

ABSTRACT

A battery thermal management system (BTMS) plays a significant role in an electric vehicle (EV)'s battery pack to avoid the adverse effect of extreme heat being generated during application. A heat pipe-based BTMS is regarded as an alternative technique to maintain an optimum working temperature of the lithium-ion batteries (LIBs) used in EVs. In this study, the heat pipe-based BTMS was designed and experimented under high input power. The battery surrogate was sandwiched with L- and I-shaped heat pipes, and heated at 30, 40, 50 and 60 W. The heat pipes' condenser sections were cooled by water at 0.0167, 0.0333 and 0.05 kg/s. Findings revealed that the designed heat pipe-based BTMS could give the maximum temperature (T_{max}) below 55 °C, even at the highest input power, and provide the temperature difference (ΔT) below 5 °C. It exhibited capability to transfer more than 92.18% of the heat generated. Controlling the T_{max} and ΔT within the desirable range demonstrates that the heat pipe-based BTMS is viable and effective at higher heat loads.

1. Introduction

Electric vehicles (EVs) have gained much attention as a promising solution against the rising world's crises, such as global warming [1], the energy crisis, air pollution, etc. The increasing popularity of EVs is strongly assisted by the lithium-ion battery (LIB) technology, which provides clean and dense energy for vehicle propulsion. Many of the attractive features of LIBs include high current, power, energy density [2], prolonged life cycle, no memory effect, and low self-discharge rate [3,4]. Despite the LIBs desirable features that led to its widespread popularity in the market, temperature is sensitive to the LIB's operation. When the temperature goes beyond a specified limit, it adversely affects LIB performance, triggers an exothermic reaction and eventually later fire and explosion. The real-world failure of LIBs in different areas of applications have been reported in Chombo and Laoonual [5] and Sun et al. [6]. LIB heating is an inevitable phenomenon; it emerges during operations and should not be underestimated [7]. Thus, an effective and efficient BTMS is crucial to ensure that LIBs are safely operated within the desired temperature and provide an acceptable temperature variation. Additionally, factors such as weight, cost, volume, dependent power and adaptability to EVs are necessary for BTMS's practical application. In a few decades, researchers have explored various BTMS techniques based on air cooling [8], liquid cooling [9], phase change materials [9], heat pipe cooling [10], nanomaterials and combinations [11,12] to control the heat generation in LIBs.

The air cooling method is less complicated, inexpensive and simple to implement. Airflow, battery layout and cooling channel size

* Corresponding author. King Mongkut's University of Technology Thonburi, Bangmod, Bangkok, Thailand.
E-mail address: somchai.won@kmutt.ac.th (S. Wongwises).

https://doi.org/10.1016/j.csite.2021.101029
Received 30 November 2020; Received in revised form 4 April 2021; Accepted 19 April 2021
Available online 24 April 2021
2214-157X/© 2021 Published by Elsevier Ltd. This is an open access article under the CC BY-NC-ND license (http://creativecommons.org/licenses/by-nc-nd/4.0/).

Nomenclature

C_p	Specific heat (J/kg/K)
I	Current (A)
m_w	Mass flow rate of water (kg/s)
Q	Water flow rate (m^3/s)
Q_w	Heat transferred to water (W)
Q_{in}	Heat generation rate (W)
T	Temperature (°C)
ΔT	Temperature difference (°C)

Subscripts

in	inlet
out	outlet
max	maximum
min	minimum
w	water

are the critical parameters for analyzing the effectiveness of the air-based BTMS. Yu et al. [13] studied the transient behavior of a staggered-arranged LIB pack under natural and forced air BTMS. They revealed that natural cooling is capable of maintaining the T_{max} and ΔT in a moderate charge/discharge rate. The forced cooling with longitudinal airflow remarkably improved thermal behavior at a flow rate of 0.8 m/s and a charging rate of 1C. Yang et al. [14] incorporated a radiator with the bionic surface structure on a cylindrical LIB pack with axial air cooling and found that a flow rate higher than 0.8 m/s could maintain the T_{max} and ΔT of the LIB module within 35 °C and 5 °C during the 3C discharge rate, respectively. Kirad and Chaudhari [15] reported the prominent effects of the BTMS's efficiency and temperature uniformity resulting from the transverse and longitudinal spacing of LIBs under a forced air cooling, respectively. Despite air-based BTMS's excellent operation, the low heat transfer coefficient [14], low thermal conductivity [11,14], substantial parasitic power consumption [11], noise and pressure drop are the major bottlenecks in modules with the vast number of LIBs operated at a high current [16], leading to uneven temperature distribution.

In contrast to the air-based BTMS, the liquid-based BTMS provides efficient cooling due to the coolants' high heat capacity [11]. The mini channel cooling system has been reported to efficiently control the LIB's heat generation [16,17]. However, the coolant volume, weight, leakages, cost and pressure drop challenge this method [17]. To complement these issues, a phase change materials (PCM) technology has been employed in BTMS to absorb and transfer heat during a solid-liquid phase transition [17]. PCM is cheap and easy to deploy in hybrid-EVs; however, it has a low heat capacity, low heat transfer and leakage when changed to a liquid phase, a lack of thermal stability, space and power requirements hinder the cooling rate.

The heat pipe is an emerging passive cooling technique with high thermal conductivity and low cost. It is lightweight, and has a long lifetime. Notably, during real-world acceleration of EVs or high charging/discharging conditions, LIBs generate heat of more than 50 W [18]. Chi and Rhi [19] conducted experiments employing an oscillating heat pipe (OHP), a battery's heating power of 20 W, and a coolant temperature of 25 °C and found that the T_{max} of the battery surface could be controlled between 50 °C and 60 °C. Amin et al. [20] observed reducing T_{max} from 45.5 °C to 37.9 °C when the heat generation per cell was 20 W, and the ambient temperature was from 26 °C to 28 °C. At the heat generation per cell of 50 W, the T_{max} was reduced from 79.1 °C to 49.9 °C. Nasir et al. [21] found that the heat pipes were capable of reducing the maximum temperature by 14.7 °C and could maintain the T_{max} of below 50 °C when the heat load was less than 10 W. Moreover, the ΔT was maintained below 5 °C when a condenser length was less than 100 mm.

Despite these excellent features, previous studies have examined the performance of the heat pipe-based BTMS with an input power of less than 50 W, whereas in the field, the heat generated goes beyond 50 W. In many studies, the maximum battery surface temperatures were achieved at low heat loads not exceeding 30 W to maintain the surface temperature of 60 °C and temperature difference within 5 °C. Therefore, to mimic the real application of LIBs, more efforts are required to maintain the maximum temperature of lower than 50 °C and temperature difference of lower than 5 °C, for heat load of more than 50 W.

In the present study, the performance of BTMS for cooling prismatic LIB with water as a cooling liquid under high input power is experimentally investigated. A battery surrogate is used instead of real NMC prismatic LIB. The L-shaped and I-shaped heat pipes are sandwiched at the top and bottom of the battery surrogate. The heat pipes were thermally interlinked on the copper holder. The performance is analyzed at various input power and water mass flow rates.

2. Experimental apparatus and procedure

2.1. Experimental setup

Fig. 1(a) shows the apparatus used in this study. It consisted of a power supply, water pump, flow meter, re-circulating bath and data acquisition system. The water was employed as a coolant, and its temperature in the re-circulating bath was maintained at 30 °C by heating or cooling with an uncertainty of ±0.5 °C. The water flow rate varied at 0.0167, 0.0333 and 0.05 kg/s with an uncertainty of

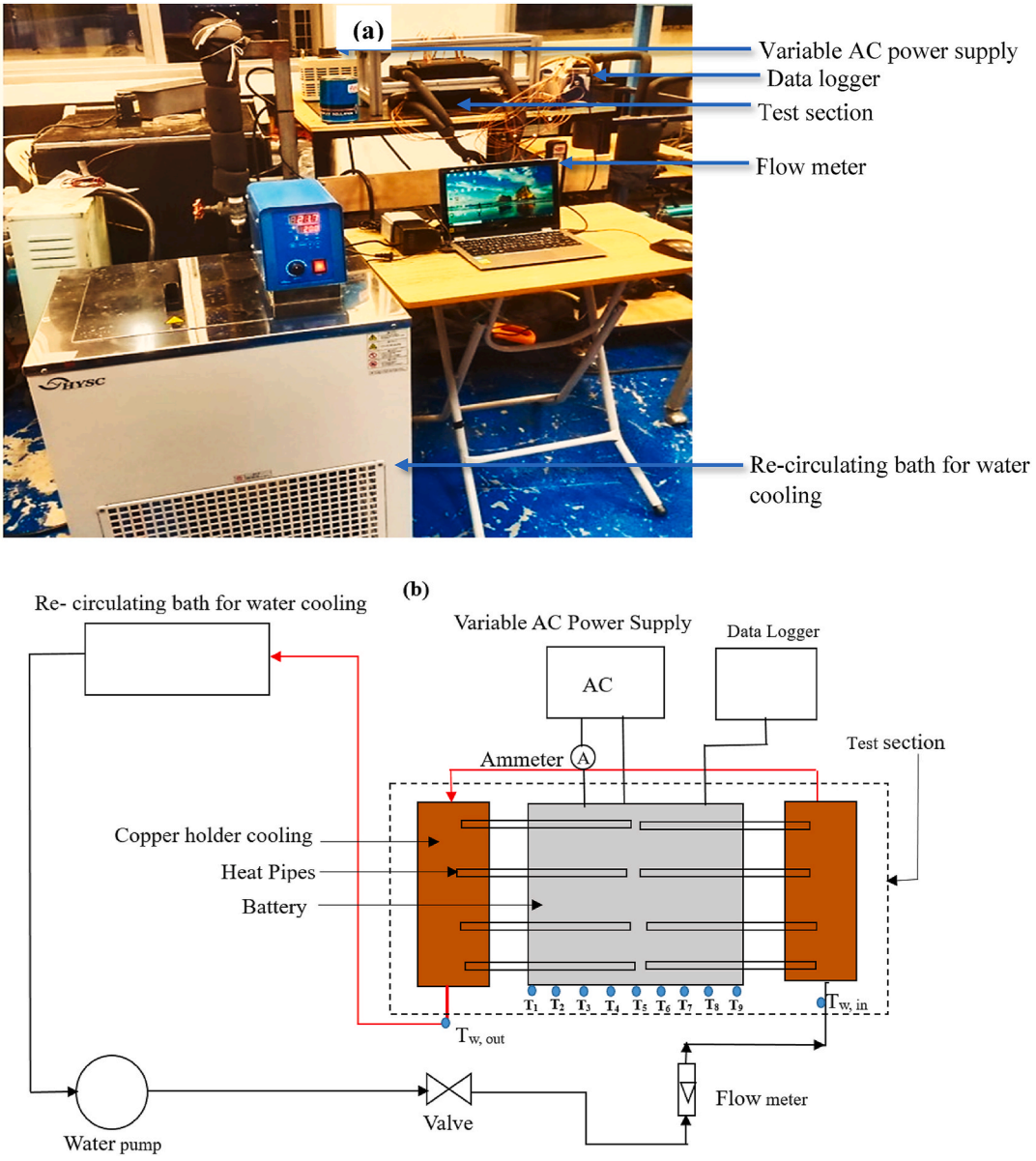

Fig. 1. (a) Photograph of the experimental apparatus (b) Schematic of the experimental set-up.

±0.001 kg/s, using a combination of the ball valve and flow meter. An aluminum ingot with thermal conductivity, which was similar to that of the LIB used in this study. Four heaters were inserted at the top of the aluminum ingot, at a depth of approximately 11 cm. The heat generation inside the battery was set to 30, 40, 50 and 60 W and was controlled by an AC power supply with an uncertainty of ±0.5 W. Nine T-type thermocouples were used to measure the battery surface temperatures, and two T-type thermocouples were set to measure the temperature of the inlet and outlet water. A data logger was used to collect temperatures from the battery surface at a sampling rate of 1 Hz using the LABVIEW program.

The test section shown in Fig. 2 (a) consisted of the aluminum plates, copper holders, and heat pipes. Aluminum plates were used to simulate batteries, and their dimensions were 173 × 125 × 45 mm. Four heaters were inserted into the four drilled holes with a 14 mm diameter at the top of the plate. The four heaters were used to generate heat.

The dimensions of the copper holder shown in Fig. 2(b) was 90 × 40 × 30 mm. It was embedded with inlet and outlet pipes having diameters of 12.7 mm. The inlet and outlet pipes circulated the coolant to and from the re-circulating bath. Fig. 2(b) shows the shapes of heat pipes mounted on the top side of the aluminum plate. Note that the aluminum plate was composed of two plates mounted side by side to form one plate. The sample of a single aluminum plate is shown in Fig. 2(c). The heat pipes shown in Fig. 2(d) were of two types, L-shaped and I-shaped. A side of L-shaped pipe with a length of 60 mm and a width of 7.5 mm, operated as a condenser, whereas another side with the length of 124 mm operated as an evaporator. On the condenser side, the heat pipe was mounted on the copper

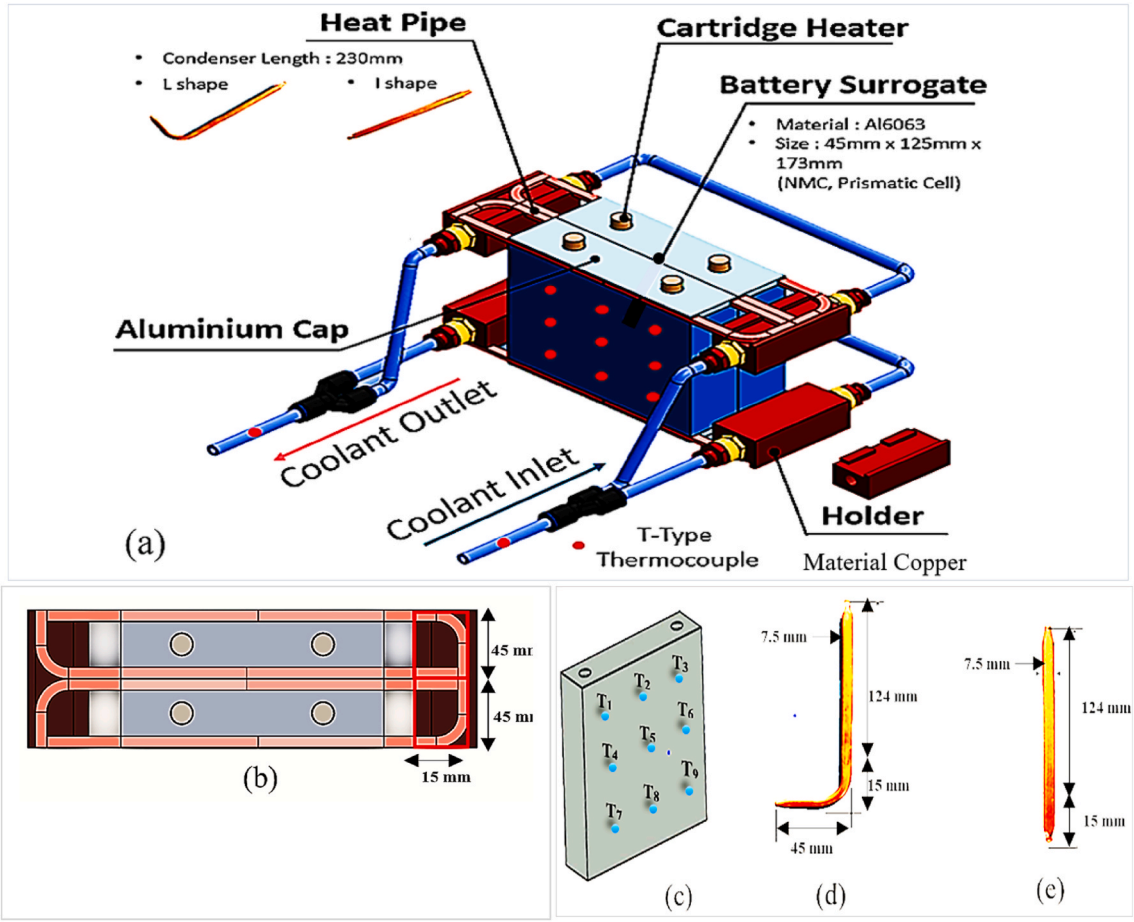

Fig. 2. (a) Test section (b) Arrangement of the heat pipe (c) Location of thermocouples on the aluminium plate (d) L-shaped heat pipe (e) I-shaped heat pipe.

holder. The I-shaped heat pipe, with a length of 124 mm, worked as an evaporator, with 15 mm working as a condenser, as shown in Fig. 2(e). The evaporator absorbed heat from the aluminum plate's surface and the condenser transferred it to the copper holder. The copper holder contained water as a cooling water and transferred the heat to the re-circulating bath. There were 8 heat pipes on the top and 8 heat pipes underneath. All heat pipes were flattened to enhance the thermal contact. Table 1 shows the specifications, Table 2 shows the accuracy of different instruments and Table 3 shows the uncertainties of the measured quantities and calculated parameters.

2.2. Experimental procedure

First, the temperature of the cooling water in the re-circulating bath was maintained at 30 °C, and then, water was allowed to circulate in the test section to ensure it was the same temperature as in the re-circulating bath. Second, the water flow rate was set to 0.0167 kg/s followed by a heater power at 30 W. Then, the data logger was triggered to record surface temperatures (T_1 to T_9) and

Table 1
Specifications of the aluminum plate equivalent to the lithium-ion battery.

Nominal capacity (Ah)	Min 94.0
	Avg. 95.6
Nominal voltage (V)	3.68
Energy (kWh)	350
Charge cut-off voltage (V)	4.15
Dimensions (mm)	173 × 125 × 45
Mass (kg)	Max. 2.06
	Avg. 2.01

Table 2
Accuracy of different instruments.

Instruments	Model	Accuracy
Dwyer mass flow meter	RMB-83D-SSV	±3%
Clamp power meter (CAT. 1000 V,600 A)	CW 10	±2.5%
Thermocouple	Omega/T-type	±0.5 °C
Cooling water bath	CWB – 30 M	±0.2 °C

Table 3
Uncertainties of measured quantities and calculated parameters.

Parameter	Uncertainty
Maximum temperature (°C)	±0.5
Coolant temperature (°C)	±0.707
Mass flow rate (kg/s)	±0.001
Temperature difference (°C)	±0.707

water temperatures ($T_{w,out}$ and$T_{w,in}$). Third, at the same water flow rate of 0.0167 kg/s, the heater power was changed to 40, 50 and 60 W; the same measurements of surface temperatures (T_1 to T_9) and water temperatures ($T_{w,out}$ and $T_{w,in}$) were then performed. Each test was conducted at approximately 2 h before the varying heater power. The experiments were then repeated by varying the water flow rate to 0.0333 kg/s and 0.05 kg/s.

3. Data reduction

In this study, the heat generation rate (Q_{in}) inside the aluminum plate depended on the input power of the heater, which could be controlled within the desired range.

$$Q_{in} = VI \tag{1}$$

where Q_{in}, V and I are the heat generation rate (W), the voltage applied to the heater (V) and the current supplied to the heater rod (A), respectively.

The heat transferred to water (Q_w) can be calculated by

$$Q_w = m_w c_p \left(T_{w,out} - T_{w,in}\right) \tag{2}$$

where m_w is the water mass flow rate (kg/s), c_p is the specific heat of water (J/kg K) and $T_{w,out} - T_{w,in}$ is the temperature difference between the inlet and outlet water (°C).

The mass flow rate is defined as follows

$$m_w = \rho Q \tag{3}$$

where Q is the water flow rate (m^3/s) and ρ is the density of water (kg/m^3).

Fig. 2(c) shows the locations for measuring the temperature on the aluminum plate. Maximum temperature (T_{max}), the minimum temperature(T_{min}) and the temperature difference ($\Delta T, T_{max} - T_{min}$) were crucial for evaluating the thermal performance of HP-BTMS [8]. For the better performance of HP-BTMS, T_{max} and ΔT were maintained below 55 °C and 5 °C, respectively.

4. Results and discussion

4.1. The effect of input power on T_{max} and ΔT

This section compares the effect of input power at a fixed flow rate and the inlet temperature of water. As seen in Fig. 3(a), the flow rate was set at 0.0167 kg/s and $T_{w,in} = 30$ °C, while the input power varied from 30 to 60 W. The maximum temperature (Tmax) and temperature difference (ΔT) were recorded to investigate the thermal behavior while varying the input power. The cooling water temperature $T_{w,out}$ was recorded to determine the amount of heat transferred.

As seen in Fig. 3(a), T_{max} in all input powers had a similar variation trend. All T_{max} rose rapidly at the initial stage of heating, and then slightly increased until reaching the steady state. The T_{max} for 30, 40, 50 and 60 W were 43.82, 46.59, 50.96 and 54.38 °C at the end of the heating process, respectively. It is clear that the T_{max} increases significantly with the input power. It should be noted that without BTMS, the T_{max} at a steady state for 30, 40, 50 and 60 W were 51.31, 57.19, 63.04 and 70.28 °C, respectively. This indicates that the designed heat pipe-based BTMS reduced the T_{max} between 7.49 °C and 15.90 °C, or 14.60%–22.62%. The temperature difference, ΔT, had the similar increasing trends. At the input power of 30, 40, 50 and 60 W, ΔT at a steady state are 2.65, 3.20, 4.07 and 4.69 °C, respectively. These ΔT show an enhancement of 25.14%–27.62%.

In Fig. 3(b), where the flow rate was set at 0.0333 kg/s, $T_{w,in} = 30$ °C and the input power varied from 30 to 60 W, the variation

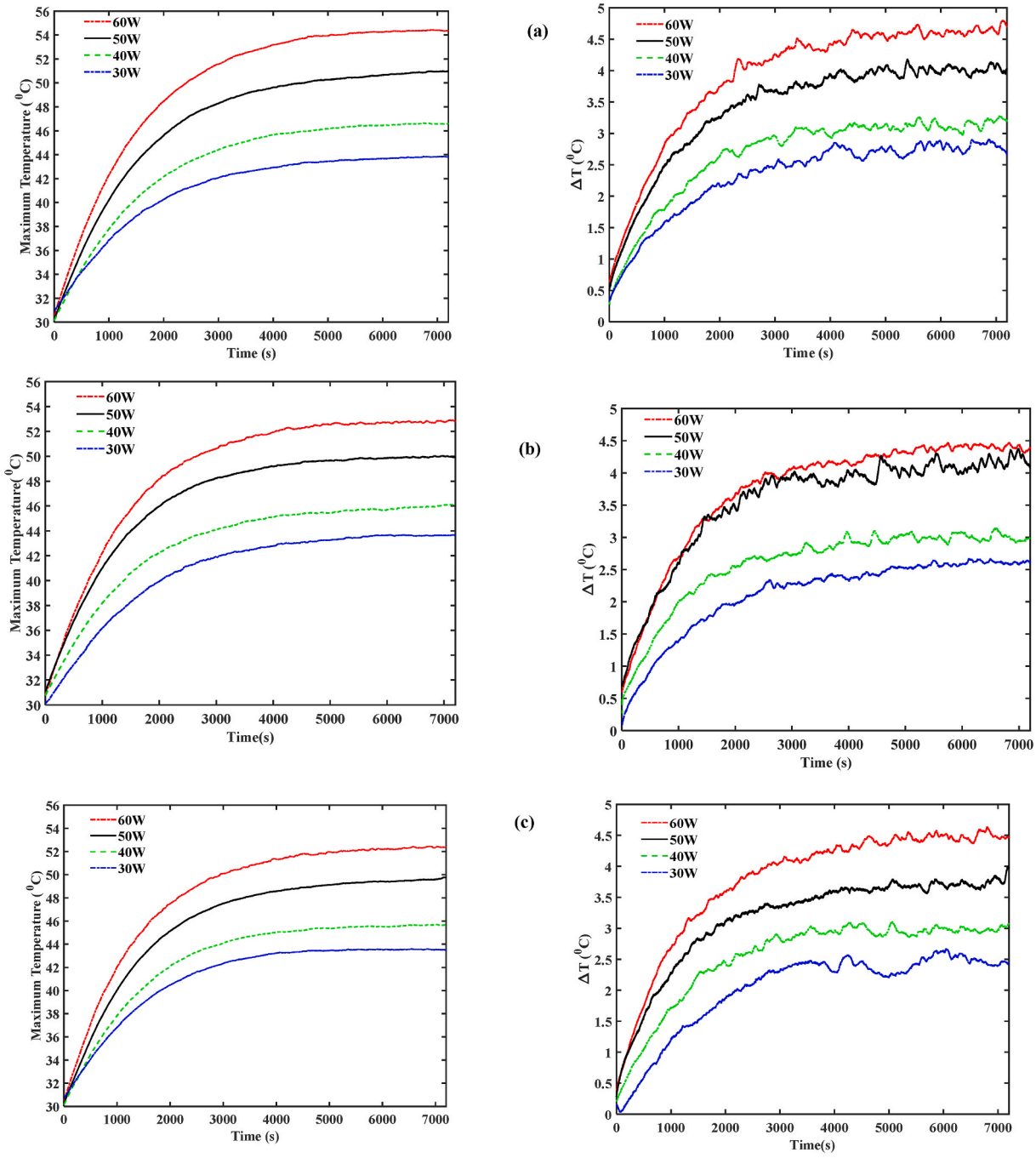

Fig. 3. T_{max} and ΔT at different input power when mass flow rate was set at (a) 0.0167 kg/s, (b) 0.0333 kg/s and (c) 0.05 kg/s.

trends of T_{max} and ΔT were similar except for the magnitude. It can be seen that the T_{max} at a steady state for 30, 40, 50 and 60 W were 43.65, 46.13, 49.93 and 52.79 °C, respectively. Compared to the T_{max} before cooling, the temperature reduction ranged between 7.66 and 17.49 °C, or 14.93%–24.89%. At this flow rate, the ΔT corresponding with the input powers was 2.61, 2.98, 4.02 and 4.38 °C, respectively. These ΔT show 26.27%–32.41% compared to the ΔT at 0.0167 kg/s.

Conversely, in Fig. 3(c), where the flow rate was 0.05 kg/s, apart from similar trends, there was only minor cooling improvement in T_{max} and ΔT. The T_{max} from Fig. 3(c) was 43.52, 45.65, 49.76 and 52.36 °C, that was only 15.18%–25.50% compared to the previous flow rate of 0.0333 kg/s. The ΔT reached 2.42, 3.07, 3.96 and 4.47 °C, respectively, which is only 31.64%–31.02%. Of great note, there was high cooling improvement from 0.0167 to 0.0333 kg/s compared to between 0.0333 and 0.05 kg/s. This elucidated that 0.0333 kg/s was the best flow rate for the optimal performance of the BTMS. It comprehensively reflects that most of the heat was transferred

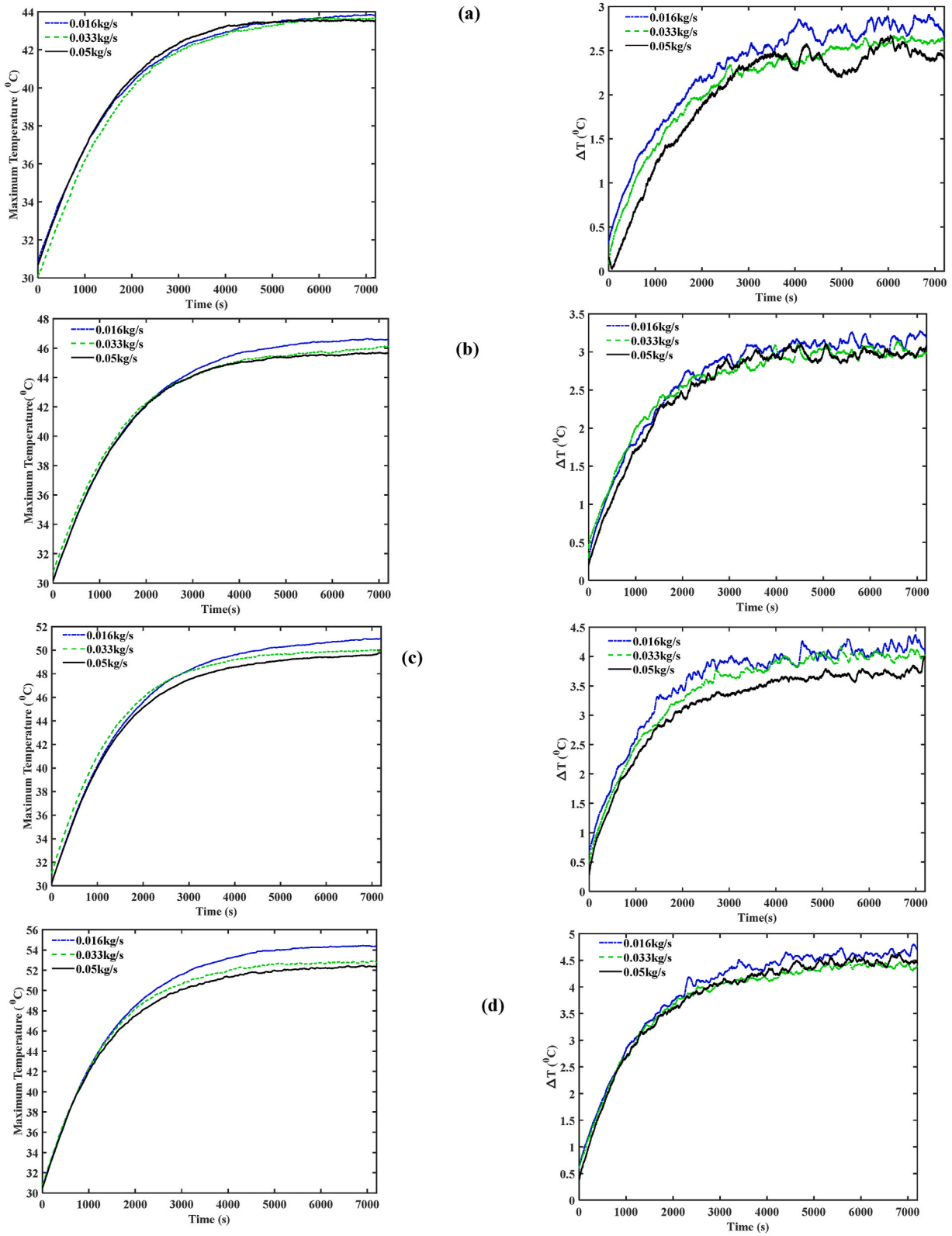

Fig. 4. T_{max} and ΔT at different mass flow rates and input power of (a) 30 W (b) 40 W (c) 50 W and (d) 60 W.

from the battery surface to the copper holder and the re-circulating bath.

4.2. The effect of water flow rate on T_{max} and ΔT

The effect of water flow rate at each input power is compared in this section. At first, the input power was set at 30 W and $T_{w,in}$ 30 °C, while the flow rate varied from 0.0167 to 0.05 kg/s. The plots of $T_{\max}$ and ΔT at different flow rates are depicted in Fig. 4(a). Later, the input power varied to 40, 50 and 60 W, while keeping $T_{w,in}$ at 30 °C. The related plots at different input powers are plotted in Fig. 4(b–d).

At the input power of 30 W, the results in Fig. 4(a) depict the similar trend in the time evolution of $T_{\max}$ at the flow rates of 0.01667, 0.0333 and 0.05 kg/s. The BTMS was able to maintain the $T_{\max}$ at 43.82 °C, a reduction of 14.6%, 14.93%, and 15.18%, respectively, in contrast to no BTMS. This corresponds to an average enhancement of 14.90%. The ΔT was maintained at 2.65 °C, a reduction of 25.14%, 26.27% and 31.64%, respectively, giving an average enhancement of 27.68%.

When increasing the input power to 40 W at a varying flow rate, $T_{\max}$ was maintained at 46.59 °C and BTMS reduced $T_{\max}$ by 18.53%, 19.34% and 20.18% (see Fig. 6(b)). This corresponds to an average enhancement of 20.34% when compared with no BTMS. From 30 W to 40 W, an average enhancement of 4.45% was achieved. The temperature uniformity ΔT was maintained at 3.20 °C, and reduced by an average of 31.17%, offsetting non-BTMS.

At the input power of 50 W (Fig. 4(c)), the $T_{\max}$ of 50.96 °C was achieved, and BTMS enhanced the cooling by 26.3%, 5.44% and 0.99% when compared with no BTMS, at 30 and 40 W, respectively. The ΔT slightly increased to about 4.07 °C, which corresponds to an average of 23.93%.

At the high input power of 60 W, the $T_{\max}$ reached 54.38 °C; which corresponds to an average enhancement of 24.34%, 9.44%, 4.99% and 4.0% in comparison with no BTMS, 30, 40 and 50 W, respectively. The ΔT reached 4.69 °C, corresponding to an enhancement of 30.35%.

4.3. The effect of input power on heat transfer rate

The heat transfer rate significantly affected the thermal performance of BTMS. To analyze this performance, the input power of 30, 40, 50 and 60 W were applied to the battery, and then water flow rates of 0.0167, 0.0333 and 0.05 kg/s were allowed to circulate through and transfer the heat off the battery.

Fig. 5 shows the effect of the input power on the heat transfer rate at different flow rates. The lowest heat transfer rate for each of the water flow rates was obtained at 30 W. As can be seen in Fig. 5, the heat transfer rates from the battery were 24.91, 25.73 and 28.86 W at the flow rates of 0.0167, 0.0333 and 0.05 kg/s, respectively. The transferred heat represented 83.03%, 85.77% and 96.20% of the heat generated, or an average of 88.33%. The better design of the heat pipes with various flow rates of cooling water resulted in the excellent longitudinal heat transfer rates of the BTMS. The concomitant is also depicted in Fig. 4, where the $T_{\max}$ and ΔT were under the desirable ranges.

Increasing the input power to 40 W raised the heat generation rate inside the battery. However, with the aid of BTMS, the heat transferred from the battery were 37.45, 37.62 and 35.12 W; reflecting 93.63%, 94.05% and 87.80%, or an average of 91.83%.

When further increasing the input power to 50 W, the heat transfer rates from the battery shot to 47.08, 48.99 and 46.56 W. The highest flow rate contributed minimally to the BTMS performance in contrast to 30 and 40 W. By raising the input power to 60 W, the BTMS performance was enhanced, which made it to an average of 93.47%.

By considering the four input powers, the trend of the heat transfer rates basically follows the input powers. To some extent, the heat transfer rate seems to be improved with the input power. For instance, at 30, 40, 50 and 60 W, the average heat transfer rate was enhanced by 88.33%, 91.83%, 95.09% and 93.47% respectively. This gave an overall heat transfer rate of 92.18%. The water flow

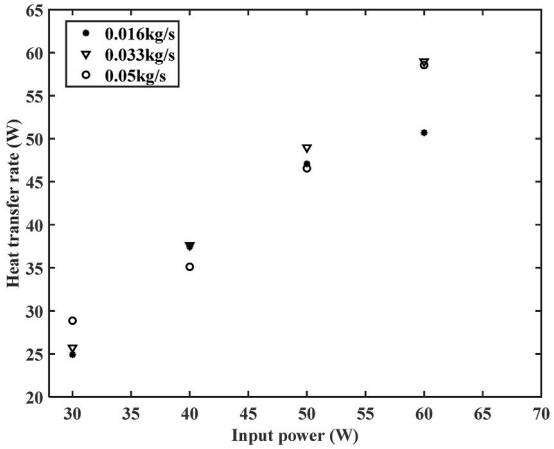

Fig. 5. Heat transfer rate at different input power.

(a)
30W
0.01067 kg/s
0.0333 kg/s
0.05 kg/s
0.016kg/s
0.033kg/s
0.05kg/s
Maximum Temperature (^{0}C)
Time (s)
ΔT (^{0}C)
Time (s)
(b)
40W
0.01067 kg/s
0.0333 kg/s
0.05 kg/s
0.016kg/s
0.033kg/s
0.05kg/s
Maximum Temperature(^{0}C)
Time(s)
ΔT (^{0}C)
Time (s)

Heat transfer rate (W)
0.0167kg/s
0.0333kg/s
0.05kg/s
Mass flow rate

Heat transfer rate (W)
0.0167kg/s
0.0333kg/s
0.05kg/s
Mass flow rate

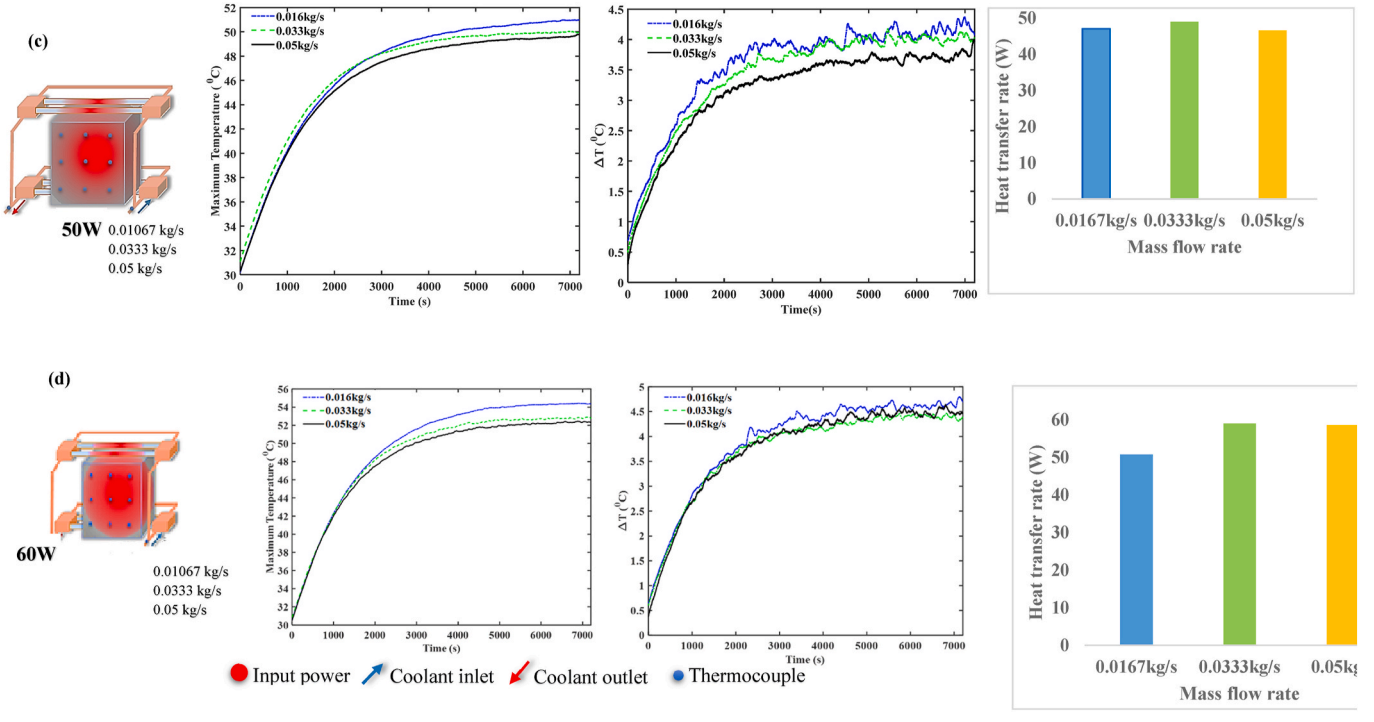

Fig. 6. Comparison between T_{max}, ΔT and heat transfer rate at different input power and flow rates.

rates at different input power varied in undefined fashion, thus giving an unclear relationship to the heat transfer rate. For example, from 30 to 40 W, the overall heat transfer rate was 10.6%, 8.28% and −8.4%; from 40 to 50 W, by 0.53%, 3.93% and 5.32%; and from 50 W to 60 W, by −9.66%, 0.32% and 4.48%. The reduced heat transfer rate with increased input power indicates the significant deterioration of the BTMS performance. The similar performance reduction behavior at the elevated input power was reported in Mei et al. [25].

However, in all scenarios, the BTMS was able to maintain the T_{max} of below 50 °C which was consistent for about 2 h. Moreover, the evenness of the temperature distribution on the battery surface slightly varied, but could be kept under the desired limit at different flow rates. Generally, better performance at high input power was observed at the highest flow rate (see Fig. 5). Note the cooling water's temperature was set to 30 °C in all conditions. So, the implication of the cooling water to the BTMS performance was not deduced. Mei et al. [25] suggested that increasing the water flow rate while decreasing its temperature could significantly reduce the T_{max} and provide the homogeneity temperature distribution on the battery's surface.

4.4. Comparison

To examine the optimum performance of the heat pipe-based BTMS, the optimum parameter, especially the flow rate, needs to be observed. Various flow rates at a steady input power were studied in terms of T_{max} and ΔT and heat transfer rate. ΔT is a crucial parameter directly affecting the temperature's evenness within the tested battery expressed as a difference between the T_{max} and T_{min} at any instant. Recent studies [22,23] reported that ΔT beyond 5 °C could form hotspots inside LIBs, which are adverse to their operation, safety and lifetime. The implication of ΔT becomes acute when unevenness emerges in the module or pack levels. To that end, many authors [22–24] have put attention on maintaining T_{max} and ΔT below 40 and 5 °C, respectively. Thus, an efficient and effective BTMS should be able to cool and keep evenness in a desirable temperature margin. To undertake a better comparison of the three flow rates and find an optimum one that can provide the best operation, the time evolution, uniformity and heat transfer are compared in Fig. 6.

As seen in Fig. 6(a–d), at the input power of 30–60 W, the BTMS at the flow rate of 0.01667 kg/s was able to control the T_{max} at 43.82–54.38 °C, ΔT at 2.65–4.69 °C, and heat transfer rate at 24.91–50.70 W. This created an enhancement of about 14.6%–22.62%, 25.14% to 27.62%, and 83.03%–84.5% when compared with no BTMS. From this condition, it is clear that increasing the input power significantly elevates the battery surface temperature and temperature homogeneity. With this low flow rate, approximately 88.83% of the heat was transferred off the battery.

Also seen in Fig. 6(a–d), by changing the flow rate to 0.0333 kg/s the T_{max}, ΔT and the heat transfer rate showed an enhancement of about 14.93%–24.89%, 26.27%–32.41%, and 85.77%–98.3% when compared with no BTMS. This flow rate had a slight improvement on T_{max}, ΔT and the heat transfer rate, particularly in lower input power. Compared to 0.05 kg/s, it is obvious that the BTMS is enhanced by 15.18%–25.5%, 31.64%–31.02%; and 96.2% (30 W) to 97.6% (60 W).

In fact, the flow rate of 0.01667 kg/s demonstrated the best performance by having the highest overall heat transfer of 94.03%, T_{max} of 52.79 °C and ΔT of 4.38 °C, which were desirable limits.

5. Conclusion

This study used heat pipe-based BTMS comprising of L-and I-shaped heat pipes utilizing water as a coolant to cool the battery when operating at higher input power. The input power from 30 W to 60 W were used to reproduce the high load at different water flow rates. The maximum surface temperature (T_{max}), temperature difference (ΔT) and heat transfer rate were examined and compared. From the results obtained, the following have been concluded:

a) The T_{max} gradually increased with the rise of input power, regardless of the flow rate. At 30, 40, 50 and 60 W, the BTMS maintained the T_{max} at 43.82, 46.59, 50.96 and 54.38 °C, respectively. Despite the high input power of 60 W, the BTMS controlled the T_{max} at below 55 °C, which satisfies the heat dissipation demand, especially at higher heat load.
b) The increasing trend of ΔT followed that of the increasing input power. At all input power, the ΔT was controlled at below 5 °C, which indicated that the designed BTMS could exhibit superior thermal management performance even at higher load.
c) The heat transfer rates' trend followed the input powers, and to some extent, it enhanced at the high input power. The overall heat transfer rate at 30, 40, 50 and 60 W was about 92.18%.

Overall, the designed BTMS exhibited the good thermal management performance for the test duration of 2 h. Despite the higher input power, about 92.18% of the heat generated was transferred by the BTMS off the battery. These findings are intriguing and promising for the future thermal management application at the module/pack level, which are extreme conditions. However, the efficiency of the BTMS will need to be further enhanced to ensure a larger heat flow rate while maintaining temperature rise and uniformity within the desirable range. Hence, this study recommends the following: the evaporator should be able to capture more heat from the battery and transfer it to the condenser; and the cooling liquid with a higher thermal conductivity and boiling temperature should be employed.

Declaration of competing interest

The authors declare that they have no known competing financial interests or personal relationships that could have appeared to

influence the work reported in this paper.

Acknowledgement

The authors would like to thank Mr. Phatsakarn Techaakarasathian, Mr. Nakapon Tapchoo and Mr. Kitsada Yongsawai for their help in constructing the experimental apparatus and collecting some data upon which this paper is based. The authors also acknowledge the financial support provided by the "Research Chair Grant" National Science and Technology Development Agency (NSTDA) and King Mongkut's University of Technology Thonburi through the "KMUTT 55th Anniversary Commemorative Fund".

References

[1] M. Kiani, M. Ansari, A.A. Arshadi, E. Houshfar, M. Ashjaee, Hybrid thermal management of lithium-ion batteries using nanofuid, metal foam, and phase change material: an integrated numerical–experimental approach, J. Therm. Anal. Calorim. 141 (2020) 1703–1715, https://doi.org/10.1007/s10973-020-09403-6.
[2] P.V. Chombo, Y. Laoonual, Investigation of the Thermal Hazard of Faulty Li-ion Battery under External Heating, International Conference and Utility Exhibition on Energy, Environment and Climate Change (ICUE), Thailand, Pattaya City, 2020, pp. 1–8, https://doi.org/10.1109/ICUE49301.2020.9307122, 2020.
[3] W. Zhang, J. Qiu, X. Yin, D. Wang, A novel heat pipe assisted separation type battery thermal management system based on phase change material, Appl. Therm. Eng. 165 (2020) 114571.
[4] P. Qin, M. Liao, D. Zhang, Y. Liu, J. Sun, Q. Wang, Experimental and numerical study on a novel hybrid battery thermal management system integrated forced-air convection and phase change material, Energy Convers. Manag. 195 (2019) 1371–1381.
[5] P.V. Chombo, Y. Laoonual, A review of safety strategies of Lithium-ion battery, J. Power Sources 478 (2020) 228649–228668.
[6] P. Sun, R. Bisschop, H. Niu, X. Huang, A review of battery fires in electric vehicles, Fire Technol. 56 (2020) 1361–1410, https://doi.org/10.1007/s10694-019-00944-3, 2020.
[7] X. Peng, X. Cui, X. Liao, A. Garg, A thermal investigation and optimization of an air-cooled lithium-ion battery pack, Energies 13 (2020) 2956, https://doi.org/10.3390/en13112956.
[8] K. Chen, M. Song, W. Wei, S. Wang, Design of the structure of battery pack in parallel air-cooled battery thermal management system for cooling efficiency improvement, Int. J. Heat Mass Tran. 132 (2019) 309–321.
[9] J. Cao, M. Luo, X. Fang, Z. Ling, Z. Zhang, Liquid cooling with phase change materials for cylindrical Li-ion batteries: an experimental and numerical study, energy 191 (2020) 116.
[10] H. Behi, D. Karimi, M. Behi, M. Ghanbarpour, J. Jaguemont, M.A. Sokkeh, F.H. Gandoman, M. Berecibar, J. Van Mierlo, A new concept of thermal management system in Li-ion battery using air cooling and heat pipe for electric vehicles, Appl. Therm. Eng. (2020) 115280.
[11] W. Yang, F. Zhou, H. Zhou, Q. Wang, J. Kong, Thermal performance of cylindrical lithium-ion battery thermal management system integrated with mini-channel liquid cooling and air cooling, Appl. Therm. Eng. 175 (2020) 115331, https://doi.org/10.1016/j.applthermaleng.2020.115331.
[12] H. Behi, D. Karimi, M. Behi, M. Ghanbarpour, J. Jaguemont, M.A. Sokkeh, F.H. Gandoman, M. Berecibar, J.V. Mierlo, A new concept of thermal management system in Li-ion battery using air cooling and heat pipe for electric vehicles, Appl. Therm. Eng. 174 (2020) 115280, https://doi.org/10.1016/j.applthermaleng.2020.115280.
[13] X. Yu, Z. Lu, L. Zhang, L. Wei, X. Cui, L. Jin, Experimental study on transient thermal characteristics of stagger-arranged lithium-ion battery pack with air cooling strategy, Int. J. Heat Mass Tran. 143 (2019) 118576, https://doi.org/10.1016/j.ijheatmasstransfer.2019.118576.
[14] W. Yang, F. Zhou, H. Zhou, Y. Liu, Thermal performance of axial air cooling system with bionic surface structure for cylindrical lithium-ion battery module, Int. J. Heat Mass Tran. 161 (2020) 120307, https://doi.org/10.1016/j.ijheatmasstransfer.2020.120307.
[15] K. Kirad, M. Chaudhari, Design of cell spacing in lithium-ion battery module for improvement in cooling performance of the battery thermal management system, J. Power Sources 481 (2020) 229016, https://doi.org/10.1016/j.jpowsour.2020.229016.
[16] X. Xu, W. Li, B. Xu, J. Qin, Numerical study on a water cooling system for prismatic LiFePO4 batteries at abused operating conditions, Appl. Energy 250 (2019) 404–412, https://doi.org/10.1016/j.apenergy .2019.04.180.
[17] Y. Huang, P. Mei, Y. Lu, R. Huang, X. Yu, Z. Chena, A.P. Roskilly, A novel approach for Lithium-ion battery thermal management with streamline shape mini channel cooling plates, Appl. Therm. Eng. 157 (2019) 113623, https://doi.org/10.1016/j.applthermaleng.2019.04.033.
[18] C. Wan, Thermal Performance of Heat Pipe Array in Battery Thermal Management 27 (2) (2020) 423–428, https://doi.org/10.17559/TV-20190731141257.
[19] R.G. Chi, S.H. Rhi, Oscilating heat pipe cooling system of electric vehicle's Li-ion batteries with direct contact bottom cooling mode, Energies 12 (2019) 1698, https://doi.org/10.3390/en12091698.
[20] M. Amin, B. Ariantara, N. Putra, A.F. Sandi, N.A. Abdullah, Thermal management of electric vehicle batteries using heat pipe and phase change materials, E3S Web of Conferences. 67 (2018), 03034, https://doi.org/10.1051/e3sconf/20186703934.
[21] F.M. Nasir, M.Z. Abdullah, M.A. Ismail, Experimental investigation on the heat transfer performance of heat pipes in cooling HEV Lithium-ion batteries, Heat Tran. Res. 49 (2018) 1745–1760.
[22] T. Amalesh, N.L. Narasimhan, Introducing new designs of minichannel cold plates for the cooling of Lithium-ion batteries, J. Power Sources 479 (2020) 228775, https://doi.org/10.1016/j.jpowsour.2020.228775.
[23] H. L Liu, H.B. Shi, H. Shen, G. Xie, The performance management of a Li-ion battery by using tree-like mini-channel heat sinks: experimental and numerical optimization, Energy 189 (2019) 116150, https://doi.org/10.1016/j.energy.2019.116150.
[24] Y. Huang, P. Mei, Y. Lu, R. Huang, X. Yu, Z. Chen, A.P. Roskilly, A novel approach for Lithium-ion battery thermal management with streamline shape mini channel cooling plates, Appl. Therm. Eng. 157 (2019) 113623, https://doi.org/10.1016/j.applthermaleng.2019.04.033.
[25] N. Mei, X. Xu, R. Li, Heat dissipation analysis on the liquid cooling system coupled with a flat heat pipe of a lithium-ion battery, ACS Omega 5 (28) (2020) 17431–17441.